# Analysis of the MOAO error budget obtained by CANARY at the WHT

F. Vidal[1a], E. Gendron[1], G. Rousset[1], T. Morris[2], M. Brangier[1], A. Basden[2], Z. Hubert[1], R. Myers[2], F. Chemla[3], A. Longmore[4], T. Butterlay[2], N. Dipper[2], C. Dunlop[2], D. Geng[2], D. Gratadour[2], D. Henry[4], P. Laporte[3], N. Looker[2], D. Perret[1], A. Sevin[1], G. Talbot[2], and E. Younger[2]

[1] LESIA, Observatoire de Paris, Universite Paris Diderot, 5 place J. Janssen, 92190 Meudon, France
[2] Durham University, Department of Physics, South Road, Durham DH1 3LE, UK
[3] GEPI, Observatoire de Paris, Universite Paris Diderot, 5 place J. Janssen, 92190 Meudon, France
[4] UKATC, Royal Observatory Edinburgh, Blackford Hill, Edinburgh, EH9 3HJ, UK

**Abstract.** CANARY is the multi-object adaptive optics (MOAO) pathfinder for the multi object IR spectrometer EAGLE proposed on the European Extremely Large Telescope (E-ELT). CANARY was installed in September 2010 on the William Herschel Telescope (WHT) Canary Islands, Spain. For the first time, MOAO correction has been demonstrated using 3 widely separated off-axis natural guide stars and one deformable mirror in open loop in a target direction. We present the detailed analysis of the fourth night of the September observation run (2010 Sep. 27th). Strehls ratios of 0.20 at $1.53\mu m$ were measured in MOAO mode while achieving 0.25 in close loop configuration (r0 = 15 cm at $0.5\mu m$). We acquired synchronized slopes from the 3 off-axis WFS and the central WFS and from these data we derive the full error budget of CANARY. We pay particular attention to the performance of the tomographic reconstruction and the open loop error. We also discuss the turbulence profile retrieved during the night that was directly measured from the instrument data in order to compute an optimized tomographic reconstruction of the on-axis wavefront.

## 1 Context

Multi Object Adaptive Optics (MOAO) concept was invented to observe simultaneously near-IR spectra of tens of high redshift galaxies spread over a very large field of view (fov) with a high angular resolution. Principle of MOAO was first presented in 2001 [Hammer 2002]. Almost 10 years after, in September 2010, the demonstrator called CANARY ([Myers 2008]), performed for the first time a MOAO correction [Gendron 2011] at the William Herschel Telescope (WHT), Canary Islands, Spain.

The goal of CANARY is to demonstrate the on-sky performance of MOAO in the perspective of the European ELT. The specifications are to perform a multidirectional AO correction in a typical fov of 5 to 10 arc minutes, in principle limited by the telescope fov by splitting the analysis path to the correction path. Unlike the others AO schemes like Single Conjugate Adaptive Optics (SCAO), Multi Conjugate AO (MCAO), or Laser Tomographic AO (LTAO), in MOAO the Wavefront Sensors (WFS) do not ”see” the Deformable Mirror (DM) leading to an open loop control scheme without any feedback. Control of the DM is blind, which adds new constrains on the DM in terms of fidelity, hysteresis, drift... New calibration scheme are also required to register the WFS position regarding the DM. WFSs are placed off-axis, on Natural (NGS) or artificial Laser Guide Stars (LGS) positions. As the WFS are much further away than to the anisoplanetic patch, the uses of tomography is required to reconstruct the wavefront on-axis using the off-axis measurements.

The main goal of the CANARY first light was to demonstrate the feasibility of the two key points: tomography prediction and open loop operation including the validation of new calibrations schemes required in open loop.

[a] fabrice.vidal@obspm.fr

## 2 CANARY system

The first phase of CANARY (called Phase A) uses 3 NGS to sense the turbulent wavefront off-axis. The optical correction is performed on-axis using one 8×8 actuator DM (total 52 actuators) plus a Tip-Tilt stage both placed in open loop on a fourth NGS direction. An IR camera is mounted after the DM to characterize the Point Spread Function (PSF) of the instrument at $\lambda = 1.53\mu m$. A fourth WFS in this on-axis channel. We call this WFS, the Truth Sensor (TS). The TS is used to measure the residual correction while the MOAO loop is running and for calibration purposes. It is also used to close the loop in SCAO mode to compare performance with the MOAO scheme.

The 4 CANARY WFS cameras are Andor EMCCD with 128×128 pixels. They are Shack-Hartmann (SH) with 7×7 subapertures with 16×16 pixels per subaperture (0.26"/pixel fov). The cameras can run at a maximum of 250Hz but for noise reduction reasons the loop frequency during the observations was set to 150Hz. A detailed overview of the bench, calibration schemes and observed asterisms is given by [Gendron 2012]. We focus on this paper on the error budget post-processed from the instrument data recorded during the night of the 27th of September 2010.

## 3 Data pipeline reduction

During the night, we alternated observations between the SCAO (closed loop on the TS), and MOAO modes (using the 3 off-axis WFS). We have Point Spread Function (PSF) IR images on the target direction (i.e the central star). In parallel to the IR images, the real-time slopes of all WFSs (off-axis and TS) plus DM voltage data were saved to determine the atmospheric parameters and evaluate the error budget. We recorded 2 types of synchronous data for all the WFS. *Engaged slopes* were recorded while the MOAO loop was engaged. It stands for open loop sensing on the 3 off-axis WFS (used to engage the loop), therefore only residual slopes are seen by the TS. *Disengaged slopes* were recorded while the MOAO loop was NOT running. DM is flattened allowing to sense the turbulence in open loop on the 4 directions.

We presents in the following the procedure we used to reconstruct different parts of the budget error of CANARY from these data.

### 3.1 IR image performance estimation

The IR images were subtracted from the background and compensated for dead pixels with a dead pixel map established on a dark image. All images were obtained using individual exposure times of 1 second, and sums of 30 images were saved. Strehl ratios (SR) have been computed on the IR images by normalizing their total energy to unity, and dividing their peak value by that of the diffraction-limited pattern sampled identically. This peak value is given by $a = \frac{\pi}{4}(D^2 - o^2)p^2/\lambda^2$ with $o$ the central obscuration diameter, and $p$ the camera pixel scale.

### 3.2 Seeing estimation

For each of the 3 off-axis WFS, $r_0$ is computed by fitting the theoretical variances of the Zernike decomposition of the Kolmogorov spectrum to the measured ones reconstructed from $Z_4$ to $Z_{36}$. As the Tip-Tilt may be polluted by the telescope tracking or vibrations of the telescope, the Tip-Tilt is excluded from the fit. $r_0$ is given at 0.5$\mu$m and at the observation angle (not rescaled to zenith).

### 3.3 CANARY error budget

Any wavefront error $\sigma_{Err}$ can be translated to the expected SR with the relation SR = exp(-$(2\pi\sigma_{Err}/\lambda)^2$) and compared to the real SR measured on the IR camera.

The error budget on the IR camera noted $\sigma^2_{ErrIR}$ can be expressed as:

$$\sigma^2_{ErrIR} = \sigma^2_{Tomo} + \sigma^2_{OL} + \sigma^2_{TomoNoiseFilt} + \sigma^2_{AliasGround} + \sigma^2_{AliasAlt} + \sigma^2_{BW} + \sigma^2_{Fit} + \sigma^2_{FieldStat} + \sigma^2_{NCPA} \quad (1)$$

From the *engaged slopes* we can measure the residual error seen by the TS noted hereafter $\sigma_{ErrTS}$. The error measured on the TS, $\sigma_{ErrTS}$, can be computed as a sum of the individual terms:

$$\sigma^2_{ErrTS} = \sigma^2_{Tomo} + \sigma^2_{OL} + \sigma^2_{TomoNoiseFilt} + \sigma^2_{NoiseTS} + \sigma^2_{AliasAltTS} + \sigma^2_{AliasAlt} + \sigma^2_{BW} + \sigma^2_{FieldStat} \quad (2)$$

Replacing Equation (2) in (1) error on the IR camera can also be expressed as:

$$\sigma^2_{ErrIR} = \sigma^2_{ErrTS} - \sigma^2_{NoiseTS} - \sigma^2_{AliasAltTS} + \sigma^2_{AliasGround} + \sigma^2_{Fit} + \sigma^2_{NCPA} \quad (3)$$

All the notations are defined hereafter in the next subsections. We describe now how we compute each of the individual terms of the error budget.

### 3.3.1 Non-Common Path Aberrations (NCPA) $\sigma^2_{NCPA}$

The best SR obtained on-bench (no turbulence) is 0.80 ± 0.02, which corresponds to a bench static aberration errors of $\sigma_{NCPA} \approx 115$ nm rms. Note that the best flat of the DM is 50 nm rms (obtained from interferometric measurements).

### 3.3.2 Field static aberrations $\sigma^2_{FieldStat}$

In MOAO, the off-axis WFS and the TS measure, in addition of the atmospheric turbulence, in-the-field static aberrations. These aberrations mainly come from the telescope and the derotator and may be different over the field. We consider them as quasi static aberrations as they slowly evolve during the night. We calibrate and subtract them in the MOAO loop. However, a non-perfect determination of the off-axis static aberrations leads to a residual static error after the MOAO correction in the on-axis direction. This on-axis static error noted $\sigma_{FieldStat}$ can be measured by the Truth Sensor by averaging its slopes measurement while the MOAO loop is engaged.

### 3.3.3 Fitting error $\sigma^2_{Fit}$

The estimation of the DM fitting error $\sigma_{Fit}$ (or undermodelling error) has been derived from the measured value of $r_0$ (see section 3.2) using the formula derived by [Conan 1994]:

$$\sigma^2_{Fit} = 0.257 N_Z^{-5/6} \left(\frac{D}{r_0}\right)^{5/3} \quad (4)$$

Considering the configuration of the WHT pupil, the central obscuration, the SH subapertures and the DM actuators geometry we have a total of 12 actuators badly seen by the WFS. Taking into account the TT stage we have a total of 52 + 2 - 12 = 42 useful actuators for the wavefront correction. [Sechaud 1999] gives the fitting error as function of the number of $n_a$ actuators in the pupil diameter:

$$\sigma^2_{Fit} = 0.335 n_a^{-5/6} \left(\frac{D}{r_0}\right)^{5/3} \quad (5)$$

Replacing $n_a = 2\sqrt{N_{tot}/\pi}$ with $N_{tot}$ the total number of actuators of the DM in Eq. (5) gives:

$$\sigma^2_{Fit} = 0.274 N_{tot}^{-5/6} \left(\frac{D}{r_0}\right)^{5/3} \quad (6)$$

and we have:

$$N_Z = \left(\frac{0.274}{0.257}\right)^{-6/5} N_{tot} \approx 0.93 N_{tot} \tag{7}$$

Using $N_{tot} = 42$ useful actuators in CANARY we have $N_Z \approx 39$ Zernikes modes to reconstructed. We have choosen the closest radial order to this value (n=7) to reconstruct $N_Z$= 36 compensated Zernike modes. In the following sections, we note $M_{iz}$ the Zernike to slopes matrix and $M_{rz}$ the slopes to Zernike reconstruction matrix (generalize inverse of the $M_{iz}$ matrix).

### 3.3.4 Bandwidth error $\sigma^2_{BW}$

The bandwidth error is computed using a set of open loop WFS data. We usually use the less noisy off-axis WFS. The signal measured by the WFS $S(t) = T(t) + n(t)$ as a sum of the turbulence term $T$ and noise $n$ (of variance $\sigma^2_{noise}$). The measured noise variance (see section 3.3.5) is used to create a noise data set from a white noise: $n(t) = \sigma_{noise} \times random\ noise(t)$.

The signal filtered by the loop $S'$ and $N'$ are computed using the openloop controller:

$$\begin{aligned} S'_t &= (1-g)S_{t-1} + g \times S_t \\ n'_t &= (1-g)n_{t-1} + g \times n_t \end{aligned} \tag{8}$$

Then, we produce a delay in the data to compute the full filtered signal by the AO system:

$$\begin{aligned} S\,filt_t &= delay \times S'_{t-1} + (1-delay) \times S'_t \\ n\,filt_t &= delay \times n'_{t-1} + (1-delay) \times n'_t \end{aligned} \tag{9}$$

The BW error is computed from the difference of the slopes variance computation of the filtered signal removed from the variance of the filtered noise term ($\sigma^2_{n-nfilt}$) to remove the noise $n$ contribution in the bandwidth estimation.

$$\sigma^2_{BW} = VAR(S_t - S\,filt_t) - VAR(n_t - n\,filt_t) \tag{10}$$

### 3.3.5 Noise error $\sigma^2_{Noise}$

We compute the slopes noise $\sigma^2_{Noise}$ from the temporal autocorrelation of slopes. At $\Delta t$=0 frames, the measured variance is the sum of the noise and turbulence variance. The turbulence variance is removed with a parabola fit of the first 2 terms ($\Delta t$=1, $\Delta t$=2) and subtracted to the value at $\Delta t$=0 to obtain the noise variance $\sigma^2_{Noise}$. The slopes noise is then propagated through the Zernike reconstruction matrix $M_{rz}$ on 36 modes ($M^2_{rz}$ denotes here all the individual coefficients of the $M_{rz}$ matrix to the square). We assume here no spatial correlation of slope noise (diagonal slope covariance matrix only).

$$\sigma^2_{Noise} = \sum_{z=1}^{36} M^2_{rz} \sigma^2_{slopesnoise} \tag{11}$$

### 3.3.6 Noise error through the tomographic reconstructor $\sigma^2_{TomoNoiseFilt}$

It is computed from the individual computation of the off-axis WFS noise propagated through the tomographic slopes reconstructor matrix called $M_t$:

$$\sigma^2_{TomoNoise} = \sum_{z=1}^{36} (M_{rz}.M_t)^2 \sigma^2_{Off-axis\ slopesnoise} \tag{12}$$

The noise really propagated by the loop is filtered by the loop gain $g$ reducing the noise variance by a factor $\frac{g}{2-g}$.

### 3.3.7 Aliasing error $\sigma^2_{Alias}$

In CANARY we used the following procedure to disentangle the different aliasing effects on the system. First, we compute the covariance matrix of the turbulence on the Zernike basis $C_{zz}$ with 900 zernikes normalized to $D/r_0 = 1$ using the formulae given by [Noll 1976]. Then, we truncate the first 36 Zernikes of the $C_{zz}$ matrix to compute the uncorrected residual Zernikes covariance matrix of the turbulence $C_{zzt}$. We project the $C_{zzt}$ matrix on the Zernike to slopes reconstruction matrix $M_{iz}$ to compute the slopes covariance matrix of the residual turbulence uncorrected by the DM noted $C_{ss}$:

$$C_{ss} = M_{iz} C_{zzt} M_{iz}^t \tag{13}$$

We finally use the Zernike reconstruction matrix $M_{rz}$ on the $C_{ss}$ slopes covariances matrix to compute the aliasing error:

$$\sigma^2_{Alias} = \sum_{z=1}^{36} \left[ Diag\left(M_{rz} C_{ss} M_{rz}^t\right) \left(\frac{D}{r_0}\right)^{5/3} \right] \tag{14}$$

As CANARY is a tomographic system we considered the aliasing effect differently as layers are in altitude or at the ground. We assume aliasing at the ground is correlated for all the WFS. This aliasing is injected in the loop and is consequently on the DM voltages and finally introduce an error on the IR camera. It not seen directly on the TS slopes but we compute its effects as a fraction of the total turbulence on the ground. We assume aliasing in altitude as a white noise not correlated between the off-axis WFS. We consider it as a noise contribution by averaging by the number of WFS and proportional to the fraction of turbulence in altitude.

### 3.3.8 Tomographic error $\sigma^2_{Tomo}$

We use a set of *disengaged slopes* to *replay* a concatenation of the off-axis slopes ($\mathbf{S}_{offAxis}$) on the tomographic reconstructor $M_t$ to compute a prediction of TS slopes. We estimate the tomographic error $\sigma^2_{Tomoraw}$ by computing in the Zernike basis the difference of the tomographic prediction and the real measurement of the turbulence made by the TS (noted $\mathbf{S}_{TS}$):

$$\sigma^2_{Tomoraw} = \sum_{z=1}^{36} (M_{rz}(\mathbf{S}_{TS} - M_t \mathbf{S}_{offaxis}))^2 \tag{15}$$

Since we compare perfectly synchronized (open loop) slopes, this error is not affected by the temporal loop filter. However, as we compare the predicted slopes to the real TS measurements we must unbias it to the TS noise $\sigma^2_{NoiseTS}$. We must also remove the noise variance from the offaxis measurements propagated into the tomographic reconstructor $\sigma^2_{TomoNoise}$. Finally, it is also needed to remove the contribution of the aliasing effect in altitude on the TS $\sigma^2_{AliasAltTS}$ and through the tomographic reconstructor $\sigma^2_{AliasAlt}$.

It comes that the pure tomographic reconstruction error $\sigma^2_{Tomo}$ is estimated using:

$$\sigma^2_{Tomo} = \sigma^2_{Tomoraw} - \sigma^2_{TomoNoise} - \sigma^2_{NoiseTS} - \sigma^2_{AliasAltTS} - \sigma^2_{AliasAlt} \tag{16}$$

We emphasize here that, on-sky, the measured $\sigma^2_{Tomo}$ term is in reality also summed up with the turbulence profile model error term $\sigma^2_{Model}$. This last term is impossible to disentangle to the pure tomographic error as the exact $C_n^2(h)$ profile is unknown and we can have only an estimation of it.

### 3.3.9 Open loop error $\sigma^2_{OL}$

The open loop error is impossible to retrieve easily from the data. While the MOAO loop is running, the TS measures the tomography summed up with the open loop error.

Nevertheless it is possible to estimate it from Eq. (2) by subtracting the measurement of the TS residual $\sigma^2_{ErrTS}$ made on-sky, with all the error terms computed individually (including $\sigma^2_{Tomo}$). *Engaged slopes* are therefore required to compute an estimation of the open loop error but also *disengaged slopes* as an estimation of the $\sigma^2_{Tomo}$ term is needed:

$$\sigma^2_{OL} = \sigma^2_{ErrTS} - \sigma^2_{Tomo} - \sigma^2_{TomoNoiseFilt} - \sigma^2_{NoiseTS} - \sigma^2_{AliasAltTS} - \sigma^2_{AliasAlt} - \sigma^2_{BW} - \sigma^2_{FieldStat} \quad (17)$$

## 4 On-sky results

We present in this section the on-sky error budget post-processed from the data recorded during the night of 27th of September 2010. We focus in particular on the 2 key points of MOAO: tomography error and open loop error. The last section presents the overall error budget computed from 3 dataset.

### 4.1 Tomographic error

Figure 1 plots the tomographic error $\sigma^2_{Tomo}$ versus the strength of the turbulence $r_0$ (see section 3.2 for $r_0$ computation). We plot the tomographic error computed from the actual MOAO tomographic reconstructor used during the on-sky operations. This reconstructor was computed using the *Learn* & *Apply* (L&A) technique from [Vidal 2010]. The *learn* step allowed us to retrieve a 3 layers $C^2_n(h)$ turbulence profile only using the instrument data while the *apply* step computed an optimized tomographic reconstructor in the on-axis (target) direction. The performance of the MOAO L&A reconstructor is represented with circles and range between 156 and 300nm rms all over the night. Since we recorded synchronous data for the 4 WFS, it is possible to replay the dataset using any other reconstructor. In particular we computed the least square error (which stand in close loop scheme as Ground Layer reconstruction or GLAO). The GLAO reconstructor range between 205 and 335nm rms. The median tomographic error all over the night in MOAO gives $\sigma_{tomoMOAO}$ =216nm rms while the GLAO reconstruction gives $\sigma_{tomoGLAO}$ =270nm rms. In average during the night, MOAO reconstruction performs 160nm rms better than the GLAO case. This is an on-sky demonstration of the advantage of the L&A optimization in the tomographic reconstruction. We emphasize again that the error computed is the sum of the pure tomographic error plus the turbulence modeling error.

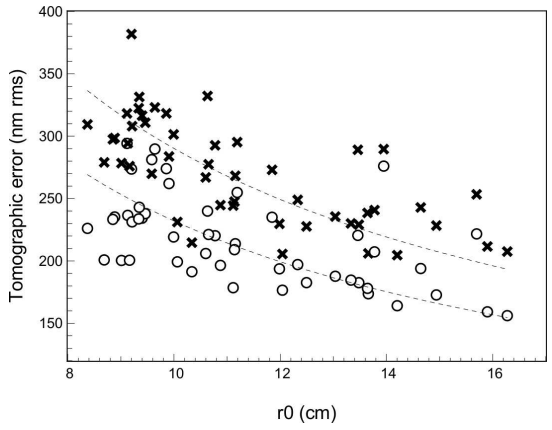


**Fig. 1.** Tomographic error measured with MOAO using the *Learn* & *Apply* technique (circles) and GLAO (crosses) reconstructor versus r0(cm). Dashed lines represents a fit by a law $\propto (D/r_0)^{5/6.}$

### 4.2 Open loop error

Figure 2 represents the open loop error as function of $r_0$. Open loop error estimation requires *engaged slopes* together with *disengaged slopes* in a short time scale. We only have 16 set of data with engaged and disengaged slopes close enough (in time) to compute a valuable error budget during the night. We estimate that open loop ranged between 160 and 55nm rms during the night. Notice that this error also include all the others unknown errors.

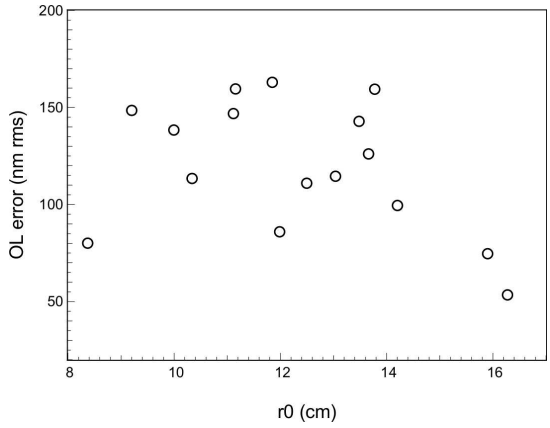


**Fig. 2.** Openloop error versus $r_0$.

### 4.3 Error budget

We present in this section the error budget computed from dataset recorded at 3 different time during the night. We have voluntarily chosen 3 different asterisms in order to be representative in the NGS geometrical configuration and $C_n^2(h)$ turbulence profile encountered during the night. Results are computed from 14 seconds of *engaged slopes* at 00h10mn12s, 03h24mn44s and 06h07mn07s respectively made on asterism #47, #53 and #12 (see [Gendron 2012] for NGS asterisms details). Few tens of seconds before, 30 seconds of IR image were recorded.

We use sets of *disengaged slopes* recorded few minutes before the engaged slopes (recorded respectively at 23h59mn, 03h14mn and 06h02mn) to separate the tomography term (including model) to the open-loop one.

Table 1 summarize the error budget retrieved from the 3 dataset. The most important term of the error budget is unsurprisingly the tomographic term. Despite the performance of the L&A tomographic reconstruction (see section 4.1) it still represents $\approx$ 27% of the total error. Others error terms in order of importance are: the fitting, the bandwidth (we remind the loop frequency was 150Hz and we measured wind speed from 6 to 8m/s), the NCPA, the open loop, the aliasing effect and noise. The field static aberrations counts for $\approx$ 6% of the total error budget. Particular effort of new calibration schemes should be envisioned to reduce this term and we emphasize here the importance of the Truth Sensor for such calibrations.

The expected SR shows a good agreement with the real SR measured by the IR camera. We respectively measured on the IR camera SR of 20.1%, 10.3% and 16.4% while the expected performance is 22.6%, 5.2% and 11.7%. We explain the difference by several factors. First, we estimate the error bars of the total error budget at $\pm$ 50nm rms leading to $\pm$4.0% error on the predicted SR. Secondly, the validity domain of the $exp(-(2\pi\sigma_{ErrIR}/\lambda)^2)$ formula tends to be pessimistic below SR of 35%. Finally, we noticed that $r_0$ fluctuated significantly on the tens of seconds between slopes and IR recordings.

**Table 1.** Error budget (in nm rms). SR are given at $\lambda = 1.53\mu m$

| Asterism | #A47 | #A53 | #A12 |
|---|---|---|---|
| *disengaged* slopes hour | 23h59mn | 03h14mn | 06h02mn |
| *engaged* slopes hour | 00h10mn | 03h24mn | 06h07mn |
| $r_0$ (cm) | 16.3 | 10.0 | 13.0 |
| $\sigma^2_{Tomo} + \sigma^2_{Model}$ | 156 | 219 | 188 |
| $\sigma^2_{OL}$ | 55 | 140 | 116 |
| $\sigma^2_{TomoNoiseFilt}$ | 48 | 56 | 97 |
| $\sigma^2_{AliasGround}$ | 95 | 132 | 83 |
| $\sigma^2_{AliasAlt}$ | 15 | 28 | 22 |
| $\sigma^2_{BW}$ | 115 | 142 | 128 |
| $\sigma^2_{Fit}$ | 138 | 206 | 165 |
| $\sigma^2_{FieldStat}$ | 77 | 106 | 72 |
| $\sigma^2_{NCPA}$ | 115 | 115 | 115 |
| **Total** $\sigma^2_{ErrIR}$ | **297** | **419** | **357** |
| Expect. SR (%) | 22.6 | 5.2 | 11.7 |
| **Meas. IR SR (%) at $\lambda$=1.53$\mu m$** | **20.1** | **10.3** | **16.4** |

## 5 Conclusion

We presented a method to process the data recorded on-sky by CANARY during the 27th of September 2010 night at the William Herschel telescope. Thanks to the presence of the Truth Sensor we were able to build a full error budget of the instrument. We evaluated 9 terms of errors including the tomographic error and the open loop error terms introduced by the MOAO scheme. The tomographic error is estimated from synchronous disengaged slopes while the open loop error requires also data when the MOAO loop is engaged. We also computed others classical AO error terms like noise, aliasing, and bandwidth errors, fitting error and NCPA.

The tomographic error ranged during the night from 156 to 300 nm rms using a tomographic reconstructor computed thanks to the Learn & Apply algorithm. The open loop error was measured between 55 and 160nm rms. We also presented the error budget computed from dataset of slopes recorded at 3 different times and geometric configurations during the night. We emphasize that the field static aberrations which are a key point of a MOAO instrument represents $\approx$ 6% of the total error measured on CANARY. Finally the expected Strehl ratio computed from the total error is close to the real SR measured by the IR camera dispite the fact that the image was recorded few tens of seconds before.

## References

[Hammer 2002] F. Hammer, F. Sayede, E. Gendron et al., In J. Bergeron & G. Monnet, editor, Scientific Drivers for ESO Future VLT/VLTI Instrumentation, page 139, (2002).

[Myers 2008] R. M. Myers, Z. Hubert, T.J. Morris et al., in SPIE proceedings, Adaptive Optics Systems. Edited by Hubin **7015** (2008)

[Gendron 2011] E. Gendron, F. Vidal, M. Brangier et al., in Astronomy & Astrophysics, Volume **529**, L2 (2011)

[Gendron 2012] E. Gendron, T. Morris, F. Vidal et al., in AO4ELT II, these proceedings (2012)

[Noll 1976] Noll, R. J., 1976, JOSA, **66**, 207

[Conan 1994] J.M. Conan, Phd thesis, Universite Paris Sud (1994) JOSA, **66**, 207

[Sechaud 1999] M. Sechaud, in Adaptive Optics in Astronomy. Cambridge University Press, Cambridge, 1999, Chap. 4, pp 57-90.

[Vidal 2010] F. Vidal, E. Gendron, and G. Rousset., Journal of the Optical Society of America A **27** (2010) pp A253 - A264.